from the last southern solstice storm to cause a value of τ comparable to that found at the current epoch.

One possible source of the current suspended soil material is a hypothetical major dust storm that occurred during the previous spring season of the northern hemisphere. (Currently it is slightly past the summer solstice in the northern hemisphere.) However, earth-based polarimetric observations of Mars show no evidence for dust clouds on a planetwide scale from December 1975 to early May 1976 (*10*). Alternatively, the current optical depth could largely be due to the cumulative effect of many local dust storms during the recent past. Such a proposal is consistent with localized darkenings observed in Mariner 9 images subsequent to the decline of the great dust storm of 1971 (*11*), and with evidence for more recent localized dust storms obtained from polarization measurements of Mars made by a Franco-Soviet experiment aboard the 1974 orbiters of the Mars series (*12*).

THOMAS A. MUTCH
Department of Geological Sciences, Brown University, Providence, Rhode Island 02912
RAYMOND E. ARVIDSON
McDonnell Center for the Space Sciences, Department of Earth and Planetary Sciences, Washington University, St. Louis, Missouri 63160
ALAN B. BINDER
Institut für Geophysik, University of Kiel, Federal Republic of Germany and *Science Applications, Inc., Pasadena, California 91101*
FRIEDRICH O. HUCK
Flight Instrumentation Division, NASA Langley Research Center, Hampton, Virginia 23665
ELLIOTT C. LEVINTHAL
Department of Genetics, School of Medicine, Stanford University, Stanford, California 94305
SIDNEY LIEBES, JR.
Department of Genetics, School of Medicine, Stanford University
ELLIOT C. MORRIS
Branch of Astrogeologic Studies, U.S. Geological Survey, Flagstaff, Arizona 86001
DAG NUMMEDAL
Department of Geology, University of South Carolina, Columbia 29208
JAMES B. POLLACK
Space Science Division, NASA Ames Research Center, Moffett Field, California 94305
CARL SAGAN
Laboratory for Planetary Studies, Cornell University, Ithaca, New York 14853

References and Notes

1. T. A. Mutch, A. B. Binder, F. O. Huck, E. C. Levinthal, S. Liebes, Jr., E. C. Morris, W. R. Patterson, J. B. Pollack, C. Sagan, G. R. Taylor, *Science* **193**, 791 (1976).
2. R. W. Shorthill, H. J. Moore, II, R. F. Scott, R. E. Hutton, S. Liebes, Jr., C. R. Spitzer, *ibid.* **194**, 91 (1976).
3. R. A. Bagnold, *The Physics of Blown Sand and Desert Dunes* (Methuen, London, 1941).
4. C. Sagan, in preparation.
5. R. E. Arvidson, M. Coradini, A. Carusi, A. Coradini, M. Fulchignoni, C. Fedrico, R. Funiciello, M. Salomone, *Icarus* **27**, 503 (1976).
6. C. Sagan, *J. Geophys. Res.* **78**, 4155 (1973).
7. ______ and R. A. Bagnold, *Icarus* **26**, 209 (1975); J. B. Pollack, R. Haberle, R. Greeley, J. Iversen, *ibid.*, in press.
8. C. Sagan and J. B. Pollack, *Nature (London)* **223**, 791 (1969); R. Greeley, B. White, R. Leach, J. Iversen, J. Pollack, *Geophys. Res. Lett.* **3**, 417 (1976).
9. O. B. Toon, J. B. Pollack, C. Sagan, *Cornell University Center for Radiophysics and Space Research Report No. 639* (1976); *Icarus*, in press.
10. E. Bowell and D. Thompson, private communication.
11. C. Sagan *et al.*, *Icarus* **17**, 346 (1972); *J. Geophys. Res.* **78**, 4163 (1973); J. Veverka *et al.*, *Icarus* **21**, 317 (1974); C. Sagan *et al.*, *ibid.*, **22**, 24 (1974).
12. A. Dollfus, private communication.
13. S. Liebes, Jr., and A. A. Schwartz, in preparation.

14. We are indebted to the following members of the Viking Lander Imaging Flight Team, who have been responsible for the preparation of imaging commands sent to the lander and for the processing of returned data: P. Avrin, C. E. Carlston, E. W. Dunham, P. L. Fox, S. U. Grenander, E. A. Guinness, K. L. Jones, R. A. Kahn, W. R. Patterson, D. C. Pieri, C. W. Rowland, R. B. Tucker, G. R. Taylor, and S. D. Wall. We are also especially indebted to R. Kahn for assistance in the atmospheric analyses. This research was supported by NASA.

2 September 1976

The "Soil" of Mars (Viking 1)

Abstract. *The location of the Viking 1 lander is most ideal for the study of soil properties because it has one footpad in soft material and one on hard material. As each soil sample was acquired, information on soil properties was obtained. Although analysis is still under way, early results on bulk density, particle size, angle of internal friction, cohesion, adhesion, and penetration resistance of the soil of Mars are presented.*

Our earlier report on physical properties (*1*) covered the first 8 sols (*2*) on Mars. This report now includes data through sol 36. The landing site of the spacecraft was characterized by two physically different "soil" types (*3*), an ideal situation for measuring differences in soil properties. Footpad 2 penetrated a soft material to a substantial depth whereas footpad 3 barely penetrated at all. Figure 1 shows a sketch map of the location of these two soil types. As a result of the normal surface sampler operations to obtain "samples" (*3*) for the biology experiment, gas chromatograph–mass spectrometer experiment (GCMS), and x-ray fluorescence experiment (XRFS), soil properties experiments were carried out. Seven trenches were dug in the surface of the so-called "Sandy Flats" and the "Rocky Flats" areas. Figure 2 shows these areas before and after acquisitions were obtained. During the delivery of the soil some of the surface material fell from the collector head of the surface sampler and was blown by the surface winds, making possible an interpretation of particle size. Images of the collector head show (Fig. 3) that soil adheres to its surface after acquisition and is partially removed after exposure to vibration and winds; this allows analysis of adhesion and depth of the surface layer. After delivery to the three active soil analysis experiments, the material remaining in the collector head was purged onto the surface. Purge site images provide yet another physical properties experiment (Fig. 4). A small comminutor or grinder is included in the GCMS processing assembly; the current drawn by the comminutor motor during grinding is recorded and provides some indication of the type of material being comminuted. A complete list of the experiments used to date to obtain estimates of soil properties is given in Table 1. We present here a brief description of the immediate environs of Viking 1 and a summary of the techniques employed to deduce these properties.

Environs. The surface in the immediate vicinity of Viking 1 consists of an area with fine-grained materials (Sandy Flats), and a rocky area set in a matrix of finer-grained material (includes Rocky Flats) (Fig. 1). Fine-grained materials, which occupy 12 to 14 percent of the sample field, were deformed by small fragments and grains propelled by rocket engine exhausts (*1*) that produced small-rimmed to rimless craters and tracks aligned along radials centered on each retro-engine (Fig. 5). Footpad 2 penetrated this material, producing open fissures and both monoclinal and anticlinal flexures of the surface near the footpad (Fig. 5). Isolated open fractures also occur several meters from the footpad; these fractures may be natural or may result from the landing. The thickness of the fine-grained material increases from the mapped boundary near the early sample sites toward footpad 2. This is further shown by the depths of trenches and the penetration of footpad 2. Some surfaces of this fine-grained material have small irregular sinuous ridges a fraction of a centimeter in diameter (Fig. 2a) that are reminiscent of "swash marks" commonly seen near the berms of beaches where spent waves have retreated back to the sea leaving a sinuous ridge of sand. These swash marks were probably formed by the deposition of fine debris entrained in retro-engine exhaust gases.

Footpad 2 is about 16.5 cm below the adjacent surface and is filled with the fine-grained material. At footpad 3 and in the region near retro-engine 3, where fines have been eroded away exposing a hard substrate, the fine-grained material is thin. Thicknesses are probably irregular in detail because the general scene has a profusion of blocks and fragments; rocks several meters away to the east protrude through the fine-grained material (*4*). Within the rocky part of the sample field, roughly 25 percent of the area is exposed rocks both on and partially beneath the surface. These rocks and exposures of rocks vary from 2 cm to several tens of centimeters in diameter. Accessible areas for sampling here are less than 25 percent because of the size of the collector head and the spacing between the rocks and rock exposures. Between rocks, fine-grained material is commonly present as thick wind tails on the south-southeast sides of rocks aligned in a southeast direction, and as thinner deposits between rocks and wind tails. Locally, these fine-grained materials have been stripped away exposing small fragments and tips of larger rocks about 0.5 cm in diameter at the surface. The general character of the rocky part of the surface probably looks the same at depth as it does at the surface.

The soils. The surface layer of Mars (*5*) can be described in terms of such properties as bulk density, particle density, particle size distribution, cohesion, adhesion, angle of internal friction, and penetration resistance. Most of the experiments listed in Table 1 provide data on more than one of these properties. For some of the soil properties a range of values is obtained. Table 2 summarizes present estimates of these properties deduced from various Viking 1 data sources. The methods used here to estimate these martian soil properties are similar to those techniques used during the lunar Surveyor Program (*6*).

Touchdown dynamics. Lander kinetic energy existing at the instant of touchdown is absorbed by the landing gear system during leg stroking, by footpad sliding and penetration into the martian surface, and by the descent engine as the thrust decays after the engine shutdown signal that is initiated at footpad contact (*1*). The effective coefficient of sliding friction developed between the footpad and martian surface material as the footpad slides laterally during leg stroking is estimated to be about 0.6; this corresponds to an angle of 31° between the normal to the footpad plane and the resultant ground reaction force. Estimates of martian penetration resistance under footpads 2 and 3 are given in Table 2. The material under footpad 2 may be a very soft layer, overlying a more competent one, such as occurs under footpad 3. It is possible, therefore, that the soil at footpad 2 is even less resistant than noted in Table 2.

Footpad penetration. Footpad 2 (Fig. 5) penetrated and possibly slid into the martian surface material a distance of 16.5 cm and is no longer visible. An arcuate depression of the surface corresponds to its perimeter. Materials have collapsed toward the footpad, filling it to a depth of 9 to 11 cm and leaving a small scarp 1 to 2 cm high and an arcuate subtle ridge some 22 cm from the edge of the footpad. Small disturbances of the surface producing monoclinal and anticlinal ridges occur up to 60 cm from the edge of the footpad. The monoclinal ridges extend to the greatest distances in the clockwise direction toward retro-engine 2. Open fractures transect these ridges. If the martian surface material fails by general shear (*7*), the geometry of the monoclinal surface deformation, the scarp, and evidence for flowage of material into footpad 2 could be explained in terms of clockwise rotation of the footpad 2 during landing as viewed in Fig. 5. Evidence of general shear is found for the footpad 2 type of material at the excavation sites where the flanks of the far end of the trenches have been domed. A question about the bulk density of the material penetrated by footpad 2 arises because the penetration is large. Such large penetrations in very fine-grained weakly cohesive materials could arise for several reasons: (i) the lower gravitational acceleration, g, on Mars; (ii) positive pore pressure resulting from the compression of the material during penetration; (iii) topographic irregularities that reduce the surface area available to resist stresses during failure

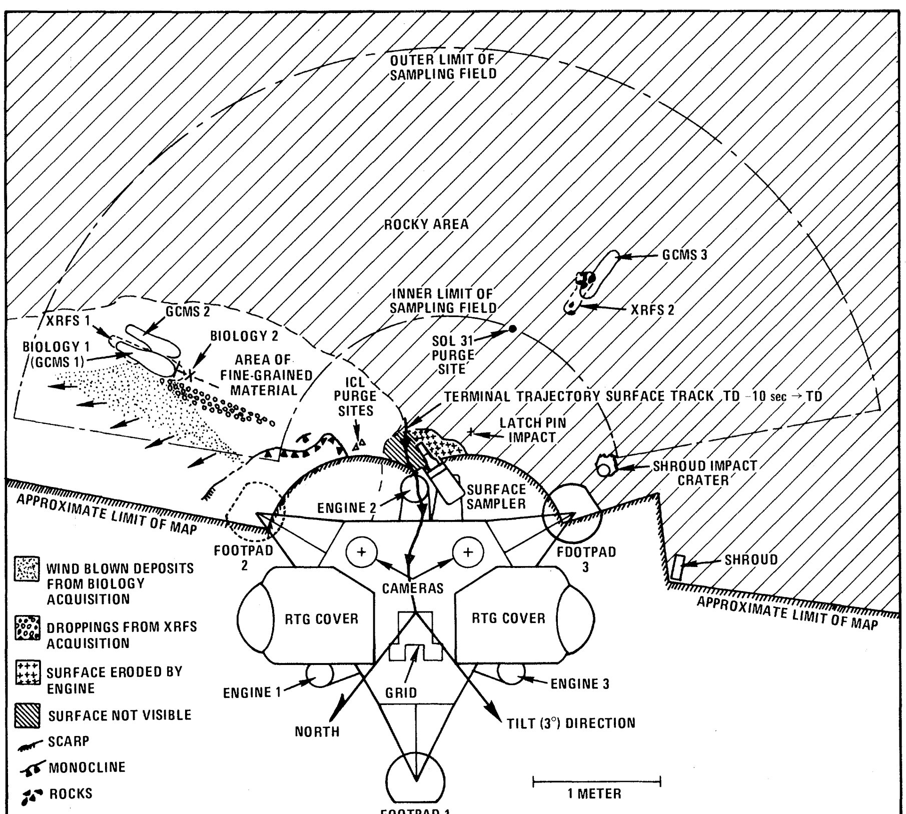

Fig. 1. Plan view of Viking 1 lander showing the spacecraft, the spacecraft orientation, salient spacecraft parts, distribution of surface materials, the location sample sites, and surface disturbances relevant to the physical properties experiment; *RTG*, radioisotope thermoelectric generator; *ICL*, initial computer load; *TD*, touchdown. Arrows near windblown deposits from the first biology experiment acquisition indicate that fines were transported beyond the mapped pattern. Acquisitions in the area of fine-grained material occurred on sol 8 and sol 14 (GCMS-2). Acquisition in rocky area for GCMS-2 occurred on sol 31. The attempted acquisition for XRFS-2 occurred on sol 34. The second acquisition for the biology experiment occurred on sol 36.

by general shear; and (iv) the topology of the penetrating object. The gravitational acceleration has been studied (*8*), and the data indicate that penetration is inversely proportional to the 0.14 power of g so that penetrations for a given rigid projectile on Mars would be 1.15 times larger than on Earth. Positive pore pressures have been assessed in small-scale experiments (*9*), which indicated that penetration was a direct function of the ambient pressure and an inverse function of the density. The effect of topography is well known (*7*). The best estimates of the local topography around footpad 2 indicate that penetration occurred on the slope of a dune-like surface which would favor a larger penetration than on a level surface. Footpad shape is important (*10*) since flat footpads penetrate less than hemispherical ones for the same mass per unit projected area and velocity. A skirt was added to the hemispherical Viking footpad for this reason. If allowances for gravitational acceleration, experimental data on ambient pressures, local topography, and footpad shape are made, empirical scaling (*11*, *12*) indicates that the resulting penetration of footpad 2 is consistent with a weakly cohesive, fine-grained material with a bulk density between 1.4 and 1.6 g/cm^2.

Wind removal of particles. After acquisition on sol 8 (Fig. 2b), a disturbed surface region was detected which extended from the near end of the sampling area back toward the spacecraft (Fig. 1). The disturbance was caused by a trail of particles falling from the collector head as it retracted after acquisition. Coarser fragments or pits caused by such fragments appear near the sampling area, and the grain size of the disturbance diminished toward the spacecraft. Upon location of the particle trail seen in the photographs on a horizontal plane through the footpads, we determined that it did not lie directly below the track of the collector head. The particle trail lay from 7.5 to 12.5 cm north of the surface projection of the track (to the left as viewed by camera 1, making allowance for spacecraft tilt). An examination of the meteorological data (*13*) for sol 8 (Table 3) shows that samples were acquired at times when the martian wind was strong, at about 10 m/sec. This wind direction is appropriate for transporting soil and rock fragments dropped from the collector head to their observed surface locations. The marks on the surface appear to be pits formed in the relatively soft soil material by falling rock fragments. It is possible to carry out some calculations to ascertain the range of sizes of rock fragments moved by the wind. The important parameter is the ratio of the lateral wind drag force to the particle weight, F/W. The particles are assumed to be spherical with radius r and a specific gravity of 2.8, appropriate to rock. The drag is not very much different if the particles are nonspherical. The drag coefficient C_D varies inversely with the Reynolds number Re of the particle in the air flow. For these particles at the recorded wind velocities, Re varies from about 10^{-2} for spheres about 1 to 2 μm in diameter up to about 10^2 for spheres a few millimeters in diameter. At low Re values, up to about $Re = 50$, the flow around the small particles is viscous and the drag coefficient is inversely proportional to the Reynolds number (*14*). Thus, under the assumed martian conditions, only the flow around the largest particles a few millimeters in diameter is just beyond the viscous regime. With this condition, from equations for the drag and weight of a spherical particle, Fig. 6 has been drawn for an assumed wind of 10 m/sec. With the surface sampler at a height of 1.0 to 1.5 m above the surface, the ratio of observed lateral drift to vertical fall of the particles dropped from the surface sampler is between 0.05 to 0.125. In Fig. 6, this number corresponds to a range of particle sizes. It can be seen that the radii of equivalent spheres vary from about 1.5 mm (0.05 ratio) to 0.9 mm (0.125).

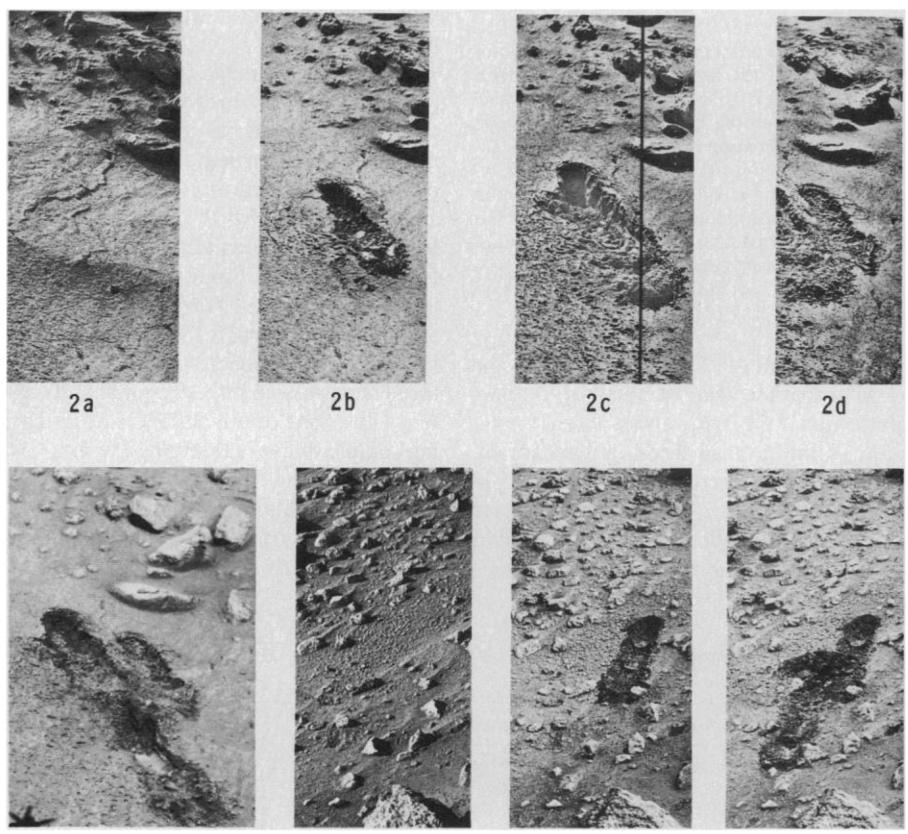

Fig. 2. Lander camera images of acquisition sites: (a) Sandy Flats before acquisition [event L.L.T. (lander local time) 008 064759 Fr 11 A 055/008; sun is from the left at an elevation angle of 17.5°]. (b) Sandy Flats acquisition trench for the biology experiment on sol 8 (event L.L.T. 008 084859 Fr 11 A 058/008; sun is from the left at an elevation angle of 43.5°). (c) Sandy Flats acquisition trench after one acquisition for the biology experiment, two acquisitions for GCMS, and two acquisitions for XRFS on sol 8 (event L.L.T. 008 141959 Fr 11 A 065/008; sun is from the right at an elevation angle of 63.0°). (d) Sandy Flats acquisition trench after a single acquisition for GCMS (GCMS-2) on sol 14 (event L.L.T. 014 101027 Fr 11 A 098/014; sun is from the left at an elevation angle of 61.7°). (e) Sandy Flats acquisition trench for the biology experiment on sol 36 (event L.L.T. 036 141441 Fr 11 B 058/036; sun is from the right at an elevation angle of 63.7°). (f) Rocky Flats before acquisition (event L.L.T. 001 074759 Fr 12 A 003/001; sun is from the left at an elevation angle of 30.0°). (g) Rocky Flats acquisition trench for GCMS on sol 31 (GCMS-3) (event L.L.T. 031 134959 Fr 12 A 243/031; sun is from the right at an elevation angle of 69.4°). (h) Rocky Flats disturbance produced during the sol 34 acquisition attempt for XRFS (XRFS-2) (event L.L.T. 034 125500 Fr 12 B 030/034; sun is from the right at an elevation angle of 81.6°). Trenches are typically 5 to 10 cm in width. Plowed material in the lower part of image is typically 9 cm in width. Fragments in the disturbed area of (h) are 2 to 4 cm. Note generally dark area in (b) which represents dynamic deposition of particles entrained by the wind and large fragments; pits and possibly clods in (c) represent droppings after the second acquisition for XRFS. Leftward displacement from the trench azimuth is due to the gravity and wind. Sinuous "swash-marks" and a subtle ridge may be seen in (a).

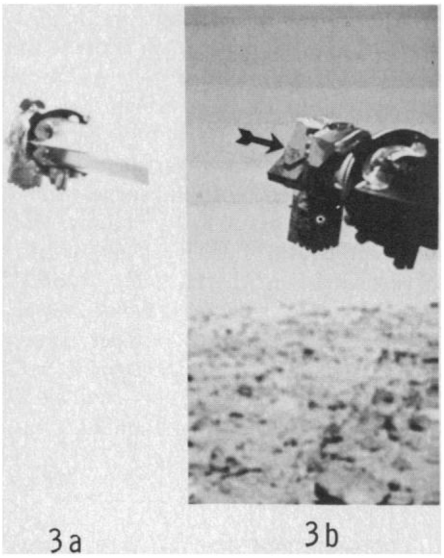

Fig. 3. Lander camera images of the collector head after: (a) the first acquisition for XRFS on sol 8 (event L.L.T. 008 104952 Fr 11 A 060/008; sun is from the left at an elevation angle of 70.1°); (b) location of the second GCMS acquisition on sol 14 (GCMS-2) (event L.L.T. 020 144959 Fr 11 A 118/020; sun is from the right at an elevation angle of 55.9°). All of the collector head is dirty in (a); there is a "highwater" (soil) mark (arrow) in (b).

We conclude, therefore, that the clearly marked trail of particles or particle impact pits lying about 10 cm to one side of the ground track of the surface sampler was caused by rock fragments in the size range of 2 to 3 mm in diameter falling off the collector head and blown to that side at the time of boom retraction. Finer sizes of particles are deflected progressively greater distances and give rise to textural or albedo differences in the martian surface farther downwind (Fig. 2c). However, if the surface disturbance is caused not by solid rock fragments but by clods or clumps of bulk density ½ to ⅓ that of the rock, then the ratio F/W (of a clod) for a given size will be two to three times that of a rock fragment. This means that, if the observed trail of disturbance was caused by soil clods instead of rock fragments, the soil clods would be about twice the rock fragment size previously estimated, or 4 to 6 mm in diameter. It seems likely that the 100 or 200 cm^3 of soil collected by the sampler contains appreciable numbers of rock fragments in the size range of a few millimeters.

Particle size. Images of the purge site (Fig. 4) when combined with other spacecraft-surface material interactions yield information on particle sizes. The largest particles observed in the two depressions produced by the purged residue from the sol 8 acquisitions are as large as 5 mm in diameter. Since the screen openings in the collector head are 2 mm in diameter, 5-mm particles would have been retained in the collector head. Finer material is possible but the frequent and violent vibrations of the collector head during sample delivery combined with a low cohesion of the fine-grained material reduce the likelihood of purging clods of fine-grained surface materials. Samples are delivered to the biology experiment through an additional 1.5-mm screen. Since material was delivered, particles smaller than 1.5 mm must be present. However, some of the material appears to be much finer because the surface became smooth and reflective when compressed and rubbed by parts of the soil acquisition hardware. This effect is illustrated by material piled up by the backhoe during retraction in the biology experiment trench (Fig. 2b), which was tamped by the boom near the pin retractor and adaptor plate. Smoothed material appears elsewhere within the biology experiment trench, the XRFS trench (Fig. 2c), and the GCMS trench (Fig. 2d).

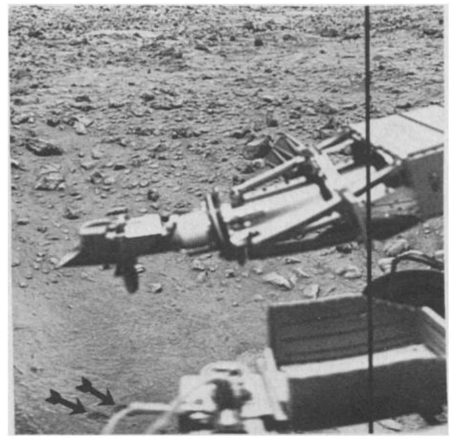

Fig. 4. Purge site for sol 8 acquisition (event L.L.T. 026 120100 Fr 11 A 149/026; sun is from the left at an elevation angle of 86.5°). There is evidence for only two purges (arrows) (out of five attempted purges); purge areas appear to be depressions, and small fragments up to 0.5 cm in diameter can be seen in the depressions.

The sol 31 GCMS acquisition trench (Fig. 2g) and sol 34 XRFS acquisition (Fig. 2h) provide data on particle size that is consistent with preacquisition expectations (Fig. 2f) that the particles are larger than at the sol 8 site. Within the GCMS trench, small clods or fragments 5 mm in diameter and smaller are visible and rocks 1 to 7 cm in diameter have been disturbed and moved. The unusually large motor currents observed during comminution in the GCMS processor are consistent with coarse cohesionless grains or granular materials. Since material delivered to GCMS passed through a 2-mm screen, it is evident that particles smaller than 2 mm are present at the sol 31 site. Fragments up to 4 cm in diameter were excavated during the XRFS acquisition. Fragments purged at a new purge site were up to 1 cm in diameter. It appears that the mean grain size of the surface material is significantly larger at the Rocky Flats sol 31 site than it was at the

Table 1. Physical properties experiments for sol 0 through sol 41. Soil properties were deduced from experiments 1, a, b, c, d; 2, a, b, c; 3, a, b, d; and 5, e.

Experiment	Measurement/observation	Derived quantities
1. Touchdown dynamics	a. Velocity vectors	Penetration resistance
	b. Stroke gauge position	Density
	c. Engine erosion	Particle size
	d. Footpad interaction	Cohesion
2. Surface impacts	a. Shroud ejection	Cohesion
	b. Boom latch pin ejection	Cohesion
	c. Purge site	Particle size
3. Surface disturbance	a. Trenches	Particle size
	b. Wind action on sample material during delivery	Particle size
	c. Rock moved	Particle size
	d. Motor current during trenching	Cohesion, friction angle
4. Comminutor	a. Motor current during grinding	Soil type
5. Environment	a. Ultraviolet-degradable coatings	Ultraviolet integrated flux
	b. Temperature sensor on footpad	Surface temperatures
	c. Temperature sensor on collector head	Surface temperatures
	d. Deposition of soil on grid during delivery	Particle size
	e. Soil adhering to lander parts	Adhesion
6. High resolution	a. Sample observed by magnification mirror	Particle size

sol 8 and sol 14 Sandy Flats acquisition sites.

Acquisition site analysis. An interactive computerized video photogrammetric system has been developed (*15*) to make possible vertical profiling and elevation contouring of the stereoscopically imaged surroundings of the lander. Figure 7 illustrates a set of vertical profiles, overlaid by the system, onto the camera 1 (left) image of the first biology experiment trench dug on sol 8. The longitudinal profiles (extending diagonally from the lower right to the upper left) are 2 cm apart; the transverse profiles (parallel to the lower edge of the image) are 5 cm apart. The central longitudinal profile (second from left in Fig. 7a) is plotted in Fig. 7b; one of the transverse vertical profiles (fifth up from the bottom in Fig. 7a) is plotted in Fig. 7c. The trench is approximately 20 cm long, 5 cm wide, and 4 cm deep. The sol 8 acquisition trenches for the GCMS and XRFS experiments were excavated to a depth of about 4 to 6 cm below the original surface (Fig. 2, a–c, and Fig. 7, a–c). The sol 14 trench (GCMS-2), which is about 12 cm closer to the boundary, was excavated to a depth of only 2.3 cm (Fig. 2d). Images of the collector head are consistent with trench depths. The collector head after the first acquisition for the XRFS experiment was everywhere covered with fine-grained material and appeared to be filled with soil (Fig. 3a) whereas the collector head image after the sol 14 acquisition (GCMS-2) had a "high-water" mark about 4.0 cm above its base, showing that the fine-grained material may be underlain by a hard substrate. A small deviation in the azimuth of the sol 8 XRFS trench to the right of that for the sol 8 biology experiment trench (for which the commanded azimuths were identical) indicates that a buried rock deflected the boom at that site. Trench walls of the sol 31 trench (GCMS-3, Fig. 2g) are knobby and similar in appearance to the surrounding surface. An acquisition on sol 34 in this area (XRFS-2, Fig. 2h) brought fragments up to 4 cm in diameter to the surface, which is consistent with the abundance of exposed rocks at the intended site. Comminutor motor currents in the GCMS processor were rather large compared to those of the sol 14 acquisition; this finding suggests that the matrix of the fines in the sol 31 sample passed easily through the 2-mm processor screens and required crushing. No such large currents were observed for the sol 14 sample of the fine-grained material that was crushed on sol 21.

The surface sampler goes through the

Table 2. Soil properties deduced from Viking 1 data (*1*). Lunar soil is included for comparison and because the nominal engineering design soil model was based on the lunar soil (*11*).

Property	Mars (Viking 1)		Lunar	
			Depth	
	Sandy Flats	Rocky Flats	0 to 0.01m	0.1 to 3 m
Bulk density (porosity) (g/cm^3)	1 to 1.6	1.8	1.0 to 1.3	1.5 to 2.1
Particle size (surface and near surface)				
~ 10 to 100 μm (%)	60	30	30 to 60	
100 to 2000 μm (%)	10	30	30 to 35	
Angle of internal friction (deg)	20° to 40°	40° to 45°	35° to 50°	
Penetration resistance ($dyne/cm^2/cm$)	3×10^4	6×10^5	3×10^5	
Cohesion ($dyne/cm^2$)	10^3 to 10^4		10^4	
Adhesion ($dyne/cm^2$)	10^1 to 10^2		10^2 to 10^3	
Coefficient of sliding friction	0.55 to 0.65		0.5 to 1	

Table 3. Summary of wind conditions on sol 8 (*6*). The motions of the surface sampler are listed as EXT, extend; UP, elevate upward; RET, retract; PURGE, empty material on surface. The azimuth of the wind is defined as the direction from which the wind is blowing.

Acquisition and purge time on sol 8				Wind		Gusts (examples)		Time span		
Hr	Minute	Second	Motion	Velocity (m/sec)	Azimuth (deg)	Velocity (m/sec)	Azimuth (deg)	Hr	Minute	Second
				Biology experiment						
7	5	57	EXT			6.3	229.6	8	36	55
7	8	21	UP	4.2	218	15.9	230.8	8	38	25
7	11	17	RET							
8	39	39	PURGE	9.25	230					
				GCMS experiment						
9	4	19	EXT			7.8	182.8	9	57	28
9	6	43	UP	9.5	222	14.2	202.5	9	58	58
9	9	39	RET							
9	32	43	EXT							
9	35	07	UP	9.5	214					
9	38	03	RET							
9	53	55	PURGE	9.6	212					
				XRFS experiment						
10	46	42	EXT							
10	49	16	UP	9.25	188					
10	54	14	RET							
11	10	48	PURGE	8.7	184					
11	33	42	EXT			3.7	154.4	11	44	49
11	36	16	UP	8.8	177	11.1	191.4	11	46	19
11	41	14	RET							
11	57	48	PURGE	8.5	168					

Table 4. Summary of forces derived from motor current readings during the extend (EXT) and retract (RET) motions of the surface sampler in the Sandy Flats area. During sample acquisition more than one attempt was sometimes made to assure that an adequate sample was collected (*7*).

Acquisition (dig)	Sol	Force (newtons)			Trench depth	Remarks
		EXT	RET			
		4 seconds	2 seconds	4 seconds		
Biology (1st)	8	0 to 22	0 to 22	0 to 8.9	~3.8 cm below original surface	Fig. 2a before acquisition; Fig. 2b after acquisition
GCMS (1st)	8	0 to 22		15.6 to 22	No image	Fig. 2c after acquisitions
GCMS (2nd)	8	0 to 17.8	15.6 to 22	0 to 4.4		
XRFS (1st)	8	0 to 4.4	11	15.6	No image	
XRFS (2nd)	8	0		13.3 to 24.4	~4 to 6 cm below original surface	
GCMS (2nd)	14	0 to 4.4	35.6	28.9	~2.3 cm below original surface	Fig. 2d after acquisition

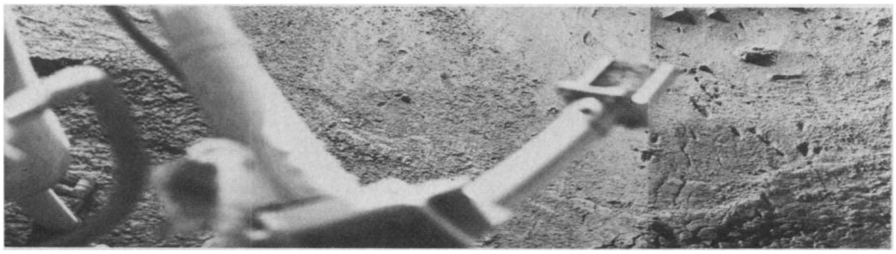

Fig. 5. Mosaic showing the area around footpad 2 (left three-quarters of the figure: event L.L.T. 012 083459 Fr 11 A 079/012; sun is from the left at an elevation angle of 40.6°; right one-quarter of the figure: event L.L.T. 004 071159 Fr 11 A 022/004; sun is from the left at an elevation angle of 22.5°). Footpad 2 is inundated by fine-grained material at the left; a subtle depression corresponding to the footpad is shown at left; a small scarp is seen at left; monoclinal and anticlinal wrinkles in the surface due to footpad deformations and open fractures are visible at the lower right. Small tracks and rimmed to rimless craters formed by particles and fragments propelled by exhaust gases from retro-engines 1 and 2 are present near the center of the mosaic.

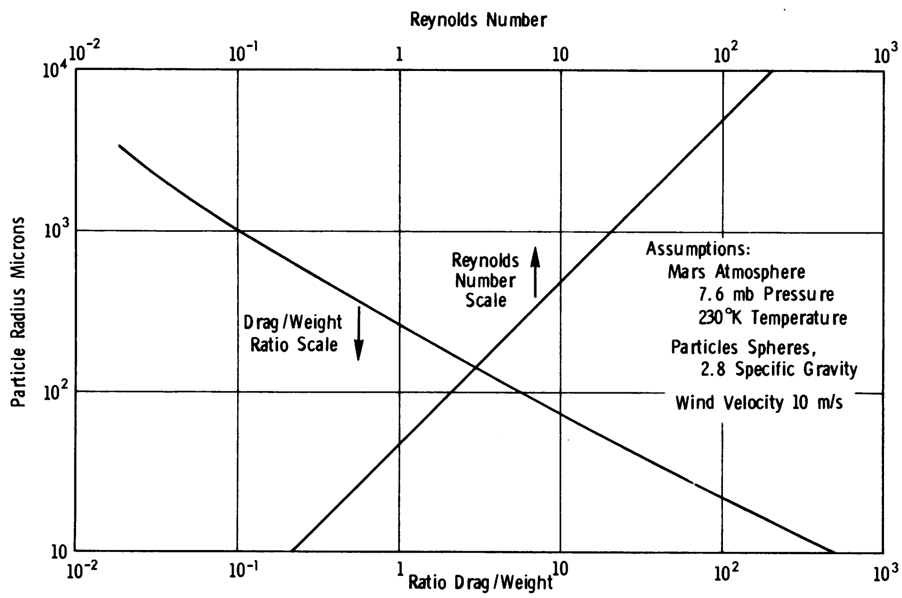

Fig. 6. Relation of particle size on Mars to the wind drag-weight ratio and *Re* during a wind of 10 m/sec.

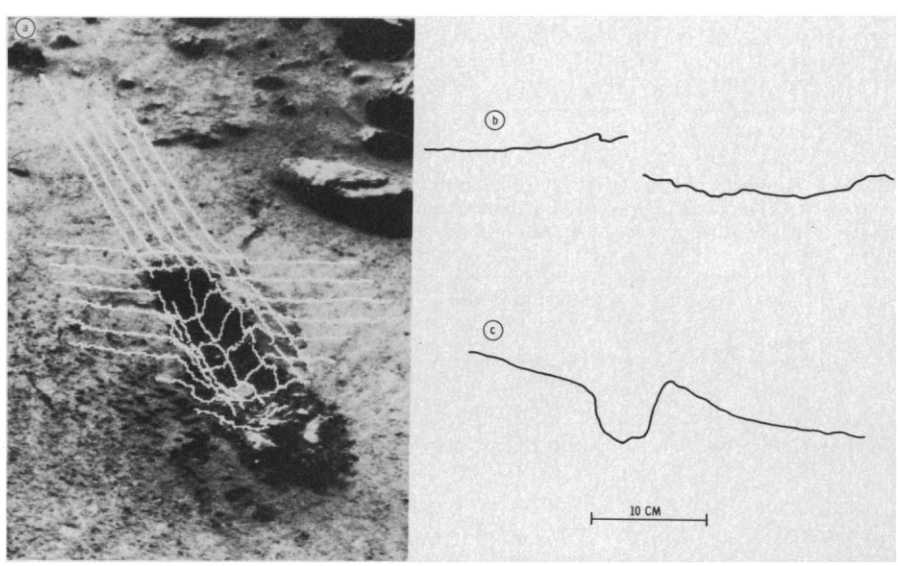

Fig. 7. (a) Vertical profiles overlaid onto camera 1 (left) image of the first biology experiment trench dug on Mars (event L.L.T. 008 064759 Fr 11 A 055/008; sun is from left at an elevation angle of 17.5°). Longitudinal profiles (extending diagonally from the lower right to the upper left) are 2 cm apart; lateral profiles are 5 cm apart. (b) Central longitudinal vertical profile [second from left in (a)] through the first trench dug on Mars. (c) Transverse vertical profile through the trench [fifth from the bottom in (a)].

following sequence of movements during acquisition: (i) extend (to the extension at which acquisition will commence); (ii) elevate down (continues until surface contact switch is actuated and stops motion); (iii) extend (in martian soil, usually a distance of 15 cm); (iv) retract (a few centimeters in soil, to make sure that the leading edge of the sampler is not under a rock); (v) elevate up (to clear surface); and (vi) retract (in martian atmosphere). Interaction of the sampler head with the martian soil occurs at the end of the first elevate down command and during extension and retraction. Motor currents required to drive the sampler are sampled twice (at 2 and 4 seconds) after the initiation of each movement. The greater the resistance to movement of the sampler, the higher the current, which can therefore be used as some measure of the resistance of the martian soil. A detailed description of motor current calibrations is found elsewhere (*16*), and only a preliminary analysis is given here. From an examination of the motor currents during the first biology experiment acquisition in sol 8 and terrestrial calibrations, we concluded that the extension peak load was in the range of 0 to 22 newtons. The retraction force deduced from the current measurements is in the range 0 to 8.9 newtons. Table 4 summarizes the forces deduced from motor currents for a number of acquisition attempts. The second dig in the GCMS acquisition on sol 14 gave an extension load that was very small, in the range of 0 to 4.4 newtons. However, in retraction, the highest motor currents recorded to date were observed. The force is estimated to be about 35.6 newtons at 2 seconds and decreased somewhat at 4 seconds to 28.9 newtons. This result is compatible with the observed shallow depth of the soil at this site, and the influence of the presence of a harder rocky substrate.

Concluding remarks. From the physical properties investigation based on the use of engineering data, lander images, and a limited amount of information from other scientific instruments, a range of soil properties was deduced. Most of the techniques used are simple, requiring minimal assumptions. It is expected that, as more refined analyses are accomplished, the values given in this report will undergo some minor revisions. More importantly, detailed analyses are required to refine these results.

During the planning and design phase of the Viking mission, a wide range of soil models was proposed (*11*) and used in the design of the spacecraft: (i) loess, (ii) dune sand, (iii) lunar nominal soil,

(iv) lag gravel, and (v) bare rock. Viking 1 successfully landed at a place that has all of these models—a credit to the engineers who designed and built the spacecraft. These materials combine to produce a scientifically interesting site.

RICHARD W. SHORTHILL
Geospace Sciences Laboratory, University of Utah Research Institute, Salt Lake City 84108
HENRY J. MOORE, II
U.S. Geological Survey, Menlo Park, California 94025
RONALD F. SCOTT
Department of Engineering and Applied Sciences, California Institute of Technology, Pasadena 91125
ROBERT E. HUTTON
Applied Mechanics Laboratory, TRW Systems Group, Redondo Beach, California 90278
SIDNEY LIEBES, JR.
Department of Genetics, Stanford University, Stanford, California 94305
CARY R. SPITZER
Viking Project Office, NASA Langley Research Center, Hampton, Virginia 23665

References and Notes

1. R. W. Shorthill, R. E. Hutton, H. J. Moore, II, R. F. Scott, C. R. Spitzer, *Science* **193**, 805 (1976).
2. "Sol" is defined as a martian day (24.6 hours). Sol 0 was 20 July 1976.
3. "Soil," as used in this report, refers to the relatively fine-grained near-surface materials of Mars that have been deformed as a result of the landing of the spacecraft and which have been acquired by the collector head. Large objects about 2 cm and larger that obviously have large cohesion are termed rocks, fragments, and blocks. The word "sample" usually indicates that which was analyzed by the three active soil analysis experiments: biology, GCMS, and XRFS. Note that GCMS-2 was not analyzed, so that GCMS-3 was the second sample analyzed by the GCMS experiment. The word "acquisition" usually refers to the process of obtaining soil.
4. T. A. Mutch, A. B. Binder, F. O. Huck, E. C. Levinthal, S. Liebes, Jr., E. C. Morris, W. R. Patterson, J. B. Pollack, C. Sagan, G. R. Taylor, *Science* **193**, 791 (1976).
5. R. W. Shorthill, R. E. Hutton, H. J. Moore, R. F. Scott *Icarus* **16**, 217 (1972).
6. R. F. Scott and F. I. Roberson, "Surveyor program results," *NASA SP-184* (1969).
7. R. F. Scott, *Principles of Soil Mechanics* (Addison-Wesley, Reading, Mass., 1963).
8. A. P. Pyrz, *Publication GSF/MC/69-6* (School of Engineering, Wright-Patterson Air Force Base, Ohio, 1969).
9. L. V. Clark, NASA Langley Research Center, letter to I. W. Ramsey, Jr., Viking Project Office, dated 12 October 1971.
10. Footpad soil penetration tests, part 1, data summary (Publication VER-188, Martin Marietta Corporation, Littleton, Colo., 1971).
11. Mars Engineering Model, Viking 75 Project Document M 75-125-3 (NASA Langley Research Center, Hampton, Va., 1974).
12. U.S. Geological Survey Interagency Report, *Astrogeology* **59**, 65 (1975); L. V. Clark and J. L. McCarty, *NASA TN D-1519* (1963).
13. S. L. Hess, R. M. Henry, C. B. Leovy, J. A. Ryan, J. E. Tillman, T. E. Chamberlain, H. L. Cole, R. G. Dutton, G. C. Greene, W. E. Simon, J. L. Mitchell, *Science* **193**, 788 (19→ S. L. Hess, R. M. Henry, C. B. Leovy, J. A. Ryan, J. E. Tillman, T. E. Chamberlain, H. L. Cole, R. G. Dutton, G. C. Greene, W. E. Simon, J. L. Mitchell, *ibid.* **194**, 78 (1976).
14. H. Schlichting, *Boundary Layer Theory* (Pergamon, New York, 1955).
15. S. Liebes and A. A. Schwartz, in preparation.
16. R. W. Shorthill, R. E. Hutton, H. J. Moore, II, R. F. Scott, C. R. Spitzer, in preparation.
17. We acknowledge the continued aid and support given to the physical properties team by the surface sampler team. The lander imaging team kindly furnished the images used in this report. The wind velocity and direction were kindly provided by the meteorology team. The help of Drs. H. Zimmer and G. Neukum during the acquisition of data is appreciated. We also thank I. M. Mack for her assistance as the physical properties intern during the month of August. We thank Dr. E. C. Morris for his continuing assistance during the Viking 1 mission and for review of the manuscript. We also thank A. Castro and V. Gillespie for their additional support. We acknowledge the help and assistance of S. Dwornik, particularly at the beginning of the project when the physical properties investigation first started. Supported by the National Aeronautics and Space Administration.

2 September 1976

Viking Orbital Colorimetric Images of Mars: Preliminary Results

Abstract. *Color reconstruction and ratios of orbital images of Mars confirm Earth-based measurements showing red/violet ratios for bright areas to be roughly 1.5 times greater than dark areas. The new results show complex variation among dark materials; dark streaks emanating from craters in southern cratered terrains are much bluer than dark materials of the north equatorial plains on which Viking 1 landed.*

The use of color in distinguishing geologic materials is applied universally at various levels. Methods vary from visual inspection, the most common, to precise measurements of spectral reflectance. During the last several years, multispectral digital imaging systems have been developed and used both in Earth-based and spacecraft programs to study and map spectral reflectivity variations on Earth, the moon, and Mercury (*1*). These systems, far more sensitive to color variation than the human eye, provide images in which the subtle color variations are related in spatial context to the regional geologic patterns and morphology. In the case of the moon, they have proved precise indicators of surface mineralogy (*2*). The Viking orbiter imaging systems have provided, for the first time, data of this nature for Mars, the most colorful of our neighboring terrestrial planets.

Spectrophotometric measurements of the reflectivity of Mars (0.3 to 2.5 μm) made from ground-based telescopes (*3*) have shown that the spectral reflectance curves of bright and dark areas are broadly separable into two types, showing different form and absorption features. Both bright and dark areas are extremely red, showing an abrupt rise in geometric albedo from 5 percent in the blue-ultraviolet to 15 to 30 percent in the red, with bright areas showing the higher red reflectance. The strong ultraviolet-blue absorption has been attributed to several percent ferric oxide in the soils (*4*). In contrast to bright areas, the dark regions display a broad absorption feature between 0.7 and 1.1 μm (*3*), which has been suggested as Fe^{2+} absorption (*5*). The mutual occurrence of Fe^{2+} and Fe^{3+} features are indicative of a thin alteration zone (< 1 μm). Further, aeolian abrasion is probably removed and disperses these thin alteration layers, exposing fresh ferrosilicate in the dark areas and depositing the fine altered material elsewhere (*4*). Although the Viking orbiter cameras have lower spectral coverage and resolution, their much higher spatial resolution allows an examination of the local geologic setting for each of the spectral types (*6*). In addition, from orbital resolution it has proved possible to recognize a greater diversity of spectral types, occurring as units too small to resolve from the earth. Finally, by comparison with surface geochemical measurements at the landing site, the orbital data provide a regional context for materials that occur there.

The Viking orbiter vidicon cameras are equipped with an array of filters covering the visible spectrum from 0.35 to 0.65 μm. Three-color images are acquired using the violet, green, and red filters (0.45 ± 0.02 μm, 0.53 ± 0.04 μm, and 0.59 ± 0.03 μm). Color scenes can be reconstructed by photometrically correcting and balancing such images to synthesize blue, green, and red components. By acquiring multiple arrays of frames in each filter, three-color mosaics are built up covering large regions. The cover illustration (this issue) is an example in which 15 frames were shuttered (five in each of the three colors). The frames were acquired over a period of about 5 minutes near apoapsis at a range of about 32,500 km to minimize variations in viewing and lighting angles < 1° among the color components.

Digital processing involved (i) removing variations in sensitivity across the fields of view to generate linear intensity scales for each frame, (ii) balancing spec-